Modeling of closed membrane shapes

Journal of Physics: Conference Series **558** (2014) 012010 doi:10.1088/1742-6596/558/1/012010

Modeling of closed membrane shapes

S Penič[1*], L Mesarec[1*], M Fošnarič[1*], V Kralj Iglič[2], S Kralj[3,4], W Góźdź[5] and A Iglič[1]

[1]Laboratory of Biophysics and Laboratory of Bioelectromagnetics, Faculty of Electrical Engineering, University of Ljubljana, Traka 25, SI-1000 Ljubljana, Slovenia
[2]Laboratory of Clinical Biophysics, Faculty of Health Sciences, University of Ljubljana, Zdravstvena 5, SI-1000 Ljubljana, Slovenia
[3]Department of Physics, Faculty of Natural Sciences and Mathematics, University of Maribor, Koroka cesta 160, SI-2000 Maribor, Slovenia
[4]Joef Stefan Institute, P.O. Box 3000, SI-1000 Ljubljana, Slovenia
[5]Institute of Physical Chemistry, Polish Academy of Sciences, Kasprzaka 44/52, 01-224 Warsaw
[*]Authors contributed equally to this work.

E-mail: samo.penic@fe.uni-lj.si, mesarec.luka@gmail.com, miha.fosnaric@fe.uni-lj.si, veronika.iglic@fe.uni-lj.si, samo.kralj@um.si, wojciech.gozdz@gmail.com, ales.iglic@fe.uni-lj.si

Abstract. Closed biological membranes were considered within the spontaneous curvature model. Ground state membrane shapes were compared with Monte Carlo simulations in the thermal equilibrium, where membranes are subject to thermal fluctuations. The results of the two approaches correspond well with each other. The oblate discocyte membrane shapes are obtained in the ground state but can become metastable when thermal fluctuations are taken into account. The nematic ordering in oblate and stomatocyte vesicle membranes was also studied. It was confirmed that the net topological charge on the surfaces with the topology of a sphere was 2. On the oblate vesicle four topological defects, each with charge 1/2, assembled in the region exhibiting the highest Gaussian curvature. On the stomatocyte vesicle with six topological defects, each with charge 1/2, and two topological antidefects, each with charge −1/2, the latter assembled in the region with a negative Gaussian curvature. The position of topological defects is strongly curvature dependent.

1. Introduction

Biological cells are enclosed by a membrane that serves as a barrier separating the interior of the cell from its surroundings [1]. Biological membranes are actively or passively engaged in trans-membrane transport, encapsulation [2, 3], communication between cells and/or cell organelles and the cell's waste control. Biological membranes are complex aggregates, composed of lipid molecules, carbohydrates, proteins and other components [4].

The main components of biological membranes are lipid molecules that are organized in a molecular bilayer [5]. The thickness of the lipid bilayer is around 5 nm, which is several orders of magnitude smaller than the lateral dimensions of the lipid vesicles or cells they enclose. This enables us to use the continuum approach in the theoretical description of membrane surfaces. Lipid bilayers in normal conditions exhibit very low resistance to bending and are therefore subject to thermal fluctuations [6].

Human erythrocytes have been intensively studied in the past. Much theoretical work has been devoted to understanding the origin of different shapes of red blood cells, such as discocytes or stomatocytes. One of the models that successfully predicted the stability these shapes is Helfrich's spontaneous curvature model [7]. Within the Helfrich's spontaneous curvature model stomatocytes and discocytes were calculated for the first time using the calculus of variation. The shapes were in good agreement with those observed in experiments.

Biological membranes can also exhibit in-plane ordering, for example lipid bilayers in regions of high curvature [8], or coated with proteins [9]. The shapes of viruses can also depend on the presence of disclinations in their protein shell [10]. A mimimal model capturing the main phenomena related to the orientational order in the membrane has been developed for colloids coated with a thin sheet of nematic liquid crystals, also referred to as nematic shells [11, 10]. Liquid crystal molecules are oriented within the tangent plane of the shell. In nematic shells with the topology of a sphere, topological defects are inevitable [12]. At the origin of topological defects, the orientational order is melted. The position of topological defects are curvature dependent [10, 13, 14, 15, 16]. On a spherical surface, the equilibrium configuration typically has four topological defects residing in vertices of a tetrahedron in order to maximize their mutual separation, which has been proved analytically [17] and confirmed experimentally [18].

In this work, we consider closed membrane surfaces with the topology of a sphere. We present different methods for studying membrane configurations we previously described in [19] and furthermore show some new, unpublished results. The paper is organized as follows. In Sec. 2, we introduce the theoretical models and briefly discuss the numerical procedures used to calculate equilibrium closed membrane shapes and nematic ordering. In Sec. 3, we present some of the results of our calculations and compare the closed membrane shapes in a ground state to those subject to thermal fluctuations. We also determine the nematic ordering on a membrane surface. In Sec. 4, we present our conclusions.

2. Models and methods

2.1. Bending energy of the membrane

Many theoretical approaches have been used in order to study the shape transformations of the closed shapes of biological membranes. In this work we used the model formulated by W. Helfrich [20] already in 1973, which treats the membrane as a homogeneous two-dimensional fluid surface characterized by the local bending energy density of the membrane in the form [7, 20, 21, 22, 23]:

$$f_b = \frac{\kappa}{2}(C_1 + C_2 - C_0)^2 + \overline{\kappa}\, C_1 C_2 \ , \tag{1}$$

where κ and $\overline{\kappa}$ are the membrane bending stiffness and saddle-splay modulus, respectively, C_1 and C_2 are the principal curvatures, and C_0 is the spontaneous curvature of the surface. Similar models were proposed by Canham [24] and Evans [21].

The overall bending energy of the membrane, F_{tot}, can be obtained by integrating Eq. (1) over the whole membrane surface:

$$F_{tot} = \int_S f_b \ \mathrm{d}S, \tag{2}$$

where $\mathrm{d}S$ is an infinitesimal element of the vesicle area S. From the Gauss-Bonnet theorem we know that the last term on the right-hand side of Eq. (1), if integrated over the closed surfaces of fixed topology, is a constant.

In the present work, we consider closed membrane shapes with the topology of a sphere. The last term on the right-hand side of Eq. (1) does not influence our shape analysis and can therefore be neglected. The bending stiffness κ of various lipid bilayers was experimentally measured (see, for example, [25], [26], [27], [28], [29], [30] and references therein).

2.2. Ground state calculations

We neglect membrane shape fluctuations due to thermal noise. We consider closed membrane shapes which are in the energy ground state and axisymmetric. To theoretically describe such shapes, we need to define the contour of the vesicle cross-section. Let the shapes be symmetric about the z-axis. The curve that defines the contour of the vesicle cross-section is rotated around the z-axis by 2π, which defines the surface of the vesicle. To describe the vesicle contour in the r-z plane, we introduce the arc length of contour s and angle, $\theta(s)$, between the tangent to the contour and the plane perpendicular to the rotation axis z. If $\theta(s)$ is known, the vesicle contour can be calculated by the following parametric equations:

$$z(s) = \int_0^s \sin\theta(s')\,\mathrm{d}s', \tag{3}$$

$$r(s) = \int_0^s \cos\theta(s')\,\mathrm{d}s', \tag{4}$$

where $r(s)$ and $z(s)$ are the coordinates of vesicle contour in r-z plane. We can express the function $\theta(s)$ in form of the Fourier series [31]:

$$\theta(s) = \frac{\theta_0}{L_s}s + \sum_{n=1}^{N} a_n \sin\left(\frac{n\pi}{L_s}s\right), \tag{5}$$

where L_s is the contour length, N is the number of Fourier modes and a_n are the Fourier amplitudes, which are calculated by minimizing the bending energy F_{tot}. If we want to restrict our calculations to the closed membrane shapes, we have to apply the following boundary conditions: $\theta(0) = 0$, $\theta(L_s) = \pi$, $r(0) = r(L_s) = 0$, which means that $\theta_0 = \pi$ in Eq. (5). The bending energy F_{tot} is basically the function of Fourier amplitudes a_n and the contour length L_s, therefore we need perform the numerical minimization of the function of many variables in order to calculate the equilibrium vesicle shapes [31, 32, 33]. In the minimization process, the constraints on the surface area and the volume of the vesicle have to be taken into account in order to ensure fixed value of the reduced volume v. The reduced volume v is defined as a ratio of the vesicle volume to the volume of the sphere with the same surface area.

2.3. Nematic shells

We have studied nematic ordering on the vesicles, which we calculated within the spontaneous curvature model as described above. We use the minimal model of in-plane ordering within vesicle membranes, which was developed to study nematic shells [11, 34]. Molecules are bound to lie in the local tangent plane of the surface. To describe the orientational ordering of molecules, we define the surface order tensor $\mathbf{Q}$. We introduce a local orthonormal basis $(\boldsymbol{e}_1, \boldsymbol{e}_2)$ in which $\mathbf{Q}$ is defined as [13, 35]:

$$\mathbf{Q} = q_0(\boldsymbol{e}_1 \otimes \boldsymbol{e}_1 - \boldsymbol{e}_2 \otimes \boldsymbol{e}_2) + q_m(\boldsymbol{e}_1 \otimes \boldsymbol{e}_2 + \boldsymbol{e}_2 \otimes \boldsymbol{e}_1),$$

where q_0 and q_m are scalar functions. In a diagonal form, tensor $\mathbf{Q}$ can be written as:

$$\mathbf{Q} = \lambda(\boldsymbol{n} \otimes \boldsymbol{n} - \boldsymbol{n}_\perp \otimes \boldsymbol{n}_\perp),$$

where λ and $-\lambda$ are eigenvalues of eigenvectors $\boldsymbol{n}$ and $\boldsymbol{n}_\perp$. Value λ is a measure for the orientational order with values in the interval $\lambda \in [0, 1/2]$. Value $\lambda = 0$ corresponds to the isotropic state with no orientational order at all, while the value $\lambda = 1/2$ corresponds to the maximal degree of the orientational order. Topological defects are points with no orientational order, therefore they usually occur where $\lambda = 0$. The basic characteristic property of the

topological defect is its topological charge [36, 35], defined as the winding number of the vector field of molecules on the tangent plane at the defect [13]. Topological charge has positive value for topological defects and negative value for topological antidefects. The theorem of Poincaré [37] states that the net topological charge is determined by a surface topology and is equal to 2 for a sphere and all surfaces obtained by smoothly deforming a sphere.

The direction of molecules and the orientational order at any given point on a vesicle can be calculated from the values of q_0 and q_m. We minimize the free energy in order to calculate the nematic ordering. In the simplest form, the dimensionless free energy density is [35]:

$$\tilde{f} = \left(\frac{R}{\xi_0}\right)^2 \left(t\ Tr\tilde{\mathbf{Q}}^2 + \frac{1}{4}\left(Tr\tilde{\mathbf{Q}}^2\right)^2\right) + \frac{1}{2}\left|\tilde{\nabla}_s\tilde{\mathbf{Q}}\right|^2, \tag{6}$$

where R is a characteristic length of the vesicle membrane and ξ_0 a nematic coherence length, which is the shortest length in the system, typically in the nanoscopic range. An ordered phase occurs below critical temperature, when t is negative. Operator $\tilde{\nabla}_s$ represents the surface gradient. In order to get the dimensionless expression for the energy density, we have scaled tensor $\mathbf{Q}$ and all the distances, which is why we used the tilde notation.

By integrating Eq. (6) over the whole surface of a vesicle membrane the total free energy is obtained and Monte Carlo method is used to minimize the total free energy. Values of $\tilde{q}_0$ and $\tilde{q}_m$ are randomly changed at random locations on the vesicle surface, until we reach the equilibrium configuration. The tilde notation denotes the scaled q_0 and q_m in the dimensionless expression for energy (Eq. (6)).

2.4. Thermal equilibrium calculations

To go beyond the ground state and model systems in the thermodynamic equilibrium, one needs to consider also thermal noise. Biological systems are often "soft enough" that thermal energy can induce important configuration changes of the system. As already mentioned in Sec. 1, lipid bilayers are, due to their low resistance to bending, subject to thermal shape fluctuations. In this section we describe the Monte Carlo simulations that take thermal fluctuations into account.

The fluid vesicle is represented by a set of N vertices that are linked by tethers (*i.e.* bonds) of variable length l in order to form a closed, randomly triangulated, self-avoiding network [38, 39]. The lengths of the tethers can vary between a minimal value, l_{min}, and a maximal value, l_{max}. The self-avoidance of the network is implemented by ensuring that no vertex can penetrate through the triangular network and that no bond can cut through another bond. In our simulations we assume $l_{max}/l_{min} = 1.7$.

The randomly triangulated network acquires its lateral fluidity from a bond flip mechanism [38, 39]. A single bond flip involves the four vertices of two neighboring triangles. The tether connecting the two vertices in a diagonal direction is cut and reestablished between the other two, previously unconnected, vertices.

The microstates of the vesicle are sampled according to the Metropolis algorithm, with the energy for a given microstate

$$E = F_{tot} - \Delta p\, V, \tag{7}$$

where the first contribution is the elastic bending energy of the vesicle (Eq. (2)) and the second contribution accounts for the energy change with the change of the volume of the vesicle, V, due to the pressure difference, Δp, inside and outside of the vesicle. Our vesicle consists of a symmetric membrane (including the absence of a mismatch between the lateral areas of the two individual membrane leaflets), therefore we do not need to include the spontaneous curvature ($C_0 = 0$). Vesicle also does not change it's topology, which means that the Gaussian bending contribution (last term on the right-hand side of Eq. (1) integrated over the vesicle surface) is constant and therefore not taken into account in our calculations. The bending energy F_{tot} of

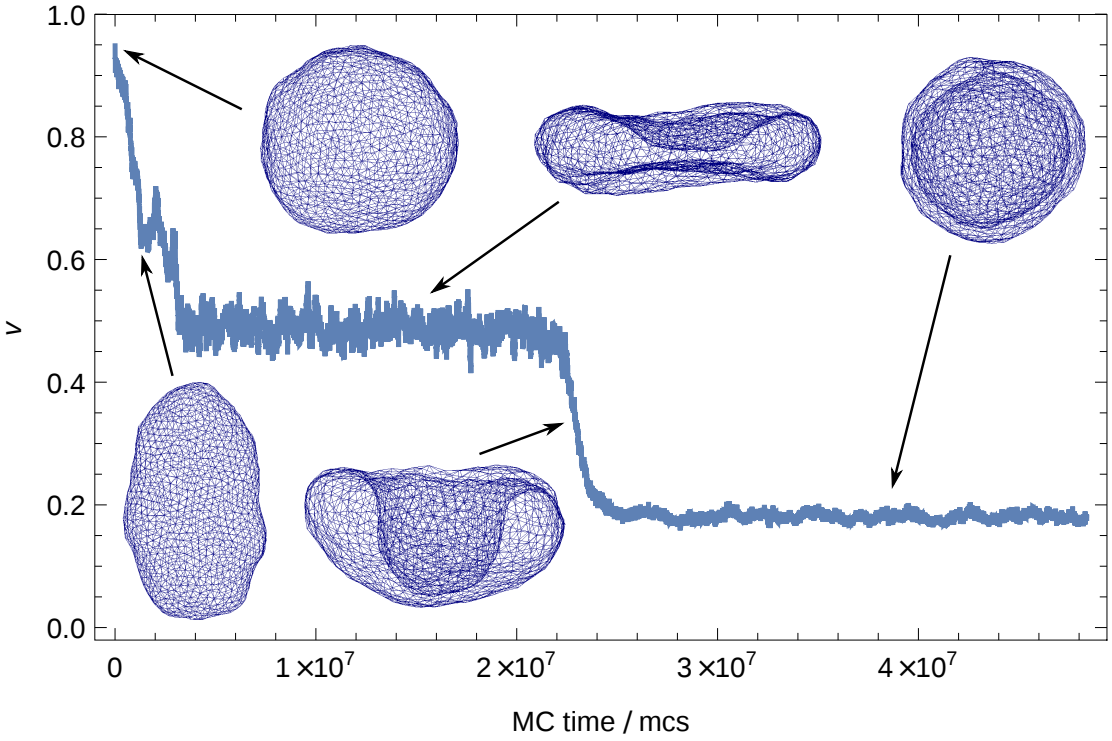

Figure 1. Monte Carlo evolution of the closed membrane vesicle from an initial quasi-spherical state towards an equilibrium stomatocyte state. The pressure difference is $\Delta p = -0.075$. The relative volume of the vesicle is presented as a function of the Monte-Carlo time (measured in mcs). The average relative volume in the equilibrium stomatocyte state is $\langle v \rangle = 0.181 \pm 0.007$, while in the metastable oblate discocyte state $\langle v \rangle = 0.50 \pm 0.02$. Above the curve, three snapshots of the vesicle are shown: the inital quazi-sphere, the discocyte and the stomatocyte. Below the curve, two snapshots of the vesicle are shown: the left configuration occurred during the transition from the quasi-sphere towards the metastable discocyte and the right configuration occurred during transition from the discocyte towards the equilibirum stomatocyte state.

the discretized vesicle (i.e., of the triangulated network) is calculated as described by Gompper and Kroll [39, 38]; for a recent review, see [40].

The evolution of the system is measured in *Monte Carlo sweeps* (mcs). One mcs consists of individual attempts to displace each of the N vertices by a random increment in the sphere with radius δ, centered at the vertex, followed by $R_{\mathrm{b}}N$ attempts to flip a randomly chosen bond. We denote R_{b} as the bond-flip ratio, which defines how many attempts to flip a bond are made per one attempt to move a vertex in one mcs. Note that the bond-flip ratio is connected to the lateral diffusion coefficient within the membrane, *i.e.* to the membrane viscosity [41, 42]. Diffusion also introduces a real time scale in the simulations and allows simulation of the dynamics of the modelled system (not considered in this work). In our simulations we have chosen $R_{\mathrm{b}} = 3$ and $\delta/l_{min} = 0.15$.

In our simulations the vesicle consists of $N = 1447$ vertices, which are connected with $3(N-2) = 4335$ bonds to form $N_{\mathrm{t}} = 2(N-2) = 2890$ triangles. The spherical vesicle has therefore a radius of approx. 13. During simulations the coordination number for each vertex (*i.e.* the number of nearest neighbors, Z) is allowed to vary between 4 and 8. For the bending stiffness of the vesicle we use $\kappa = 10\, k_B T$, where k_B is the Boltzmann constant and T the

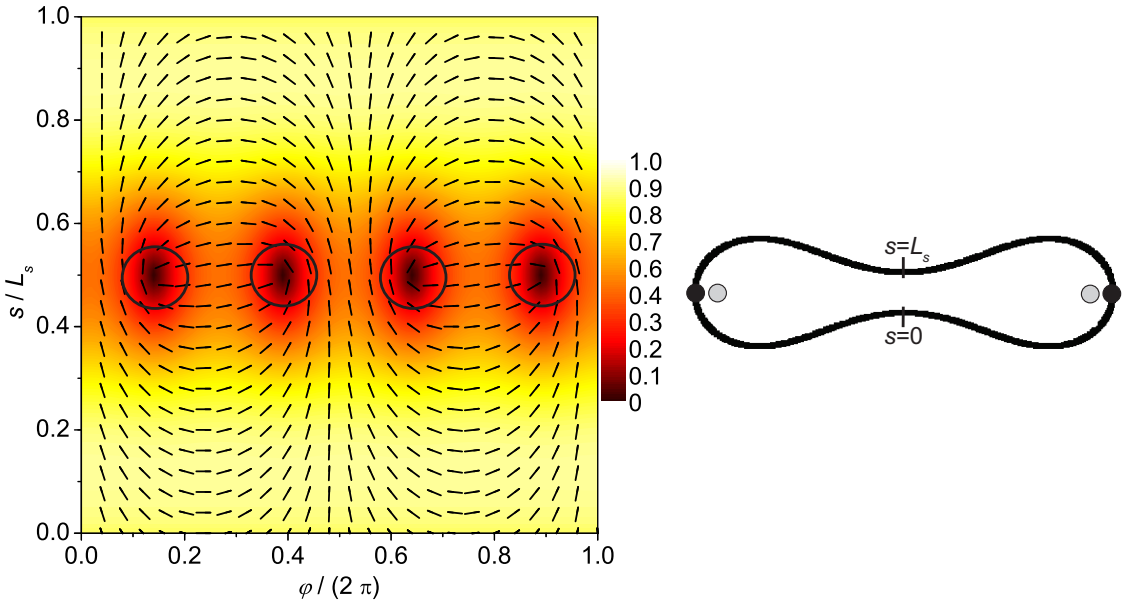

Figure 2. The calculated vector field in the membrane and contour plot of λ/λ_c ratio, where condensation value λ_c stands for the highest possible value of λ at given $t < 0$ (left panel). Configuration was calculated for $R/\xi_0 = 20$ and $t = -0.03$. The right panel shows the oblate vesicle shape with the reduced volume $v = 0.60$, calculated within the spontaneous curvature model for $C_0 = 0$. In the left panel topological defects with topological charge 1/2 are encircled with black lines. The right panel shows approximate positions of topological defects, which are represented by the black and grey dots.

absolute energy. In the following we use l_{min} as the unit length and k_BT as the unit of energy.

3. Results and Discussion

The result of minimizing the bending energy F_{tot}, as defined in Section 2, yield ground state configurations of stomatocytic, oblate and prolate shapes, each of them being the equilibrium shapes in some range of the reduced volume v, as reported in [19]. Similar results were obtained in [43, 44]. In [19] we also compared minimal energy shapes (as described in Sec. 2.2) and thermal equilibrium shapes 2.4. The method described in Sec. 2.2 allows us to set the value for the reduced volume v, so that we are able to calculate the whole spectrum of shapes for different reduced volumes. In Monte Carlo simulations we have changed the parameter Δp (inside/outside pressure difference). Once we have obtained the equilibrium state for the given Δp, we were also able to calculate the average reduced volume $\langle v \rangle$ for that state, in order to compare thermal equilibrium and ground state calculations. Thermal equilibrium states obtained by Monte Carlo simulations correspond well to the ground state shapes calculated by the minimization of the bending energy.

Ground state oblate shapes are possible only in a small region of the values of the reduced volume v. By using Monte Carlo simulations we were not able to obtain the equilibrium but only "transient" oblate shapes. Figure 1 shows the Monte Carlo evolution of the vesicle from an initial quasi-spherical towards an equilibrium stomatocyte state. As can be seen, the vesicle spends a relatively long "time" in a metastable oblate discocyte state before it reaches the equilibrium state.

We calculated the nematic ordering of the oblate vesicle membrane with the reduced volume

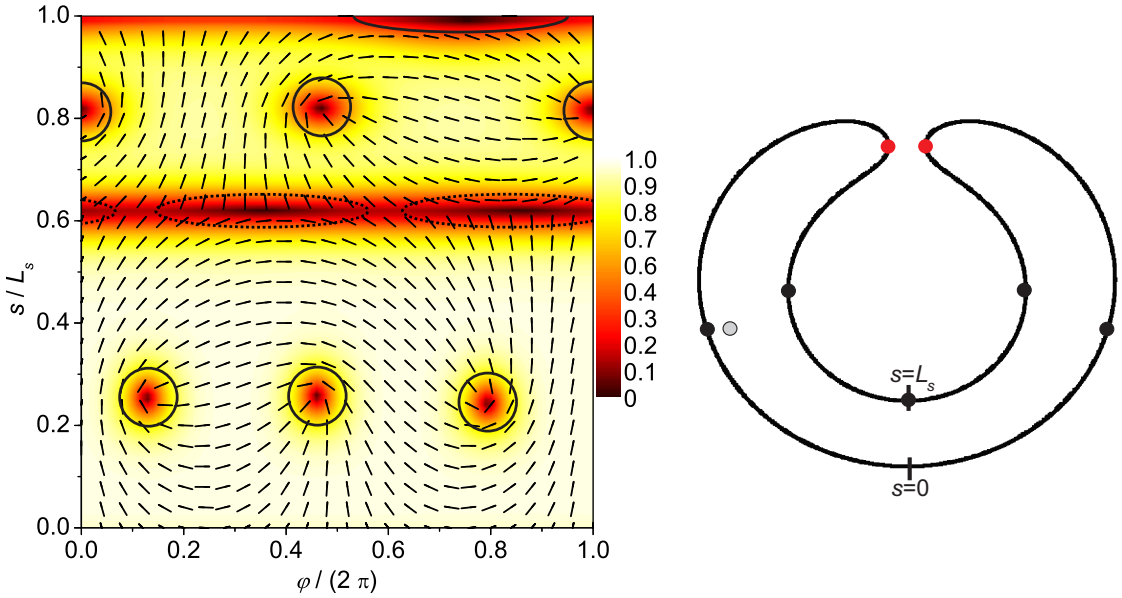

Figure 3. The calculated vector field in the membrane and contour plot of λ/λ_c ratio, where condensation value λ_c stands for the highest possible value of λ at given $t < 0$ (left panel). Configuration was calculated for $R/\xi_0 = 40$ and $t = -0.03$. The right panel shows stomatocyte vesicle shape with the reduced volume $v = 0.50$, calculated within the spontaneous curvature model for $C_0 = 0$. In the left panel topological defects with topological charge $1/2$ are encircled with black lines, while antidefects with topological charge $-1/2$ are encircled with black dashed lines. The right panel shows approximate positions of topological defects and antidefects. The black and grey dots represent topological defects, while the red dots represent antidefects.

$v = 0.60$, which was calculated within the spontaneous curvature model. In figure 2 the topological defects are points where $\lambda = 0$ (dark red color). The equilibrium configuration has four topological defects, each with charge $1/2$, which satisfies the Poincaré theorem [37]. Topological defects occur in the region of the vesicle with the highest positive Gaussian curvature. Regions of the vesicle exhibiting lower Gaussian curvature have a higher degree of orientational order (yellow color). The equilibrium configuration and the positions of topological defects are thus strongly curvature driven as previously described in [13, 16].

The nematic ordering in the membrane of the stomatocyte vesicle (figure 3) is more complex, because some of the membrane regions exhibit negative Gaussian curvature, which is favorable for topological antidefects. In the membrane regions with a negative Gaussian curvature two antidefects occur, each with topological charge $-1/2$. The stomatocyte is composed of two approximately spherical surfaces and the neck which connects them. Both spherical surfaces have a positive Gaussian curvature, while the neck region has a negative Gaussian curvature. The positive Gaussian curvature is favorable for topological defects. To this end, we can observe three topological defects on each spherical surface, each with charge $1/2$. If we sum up all topological charges on the membrane of the stomatocyte vesicle, we get the net topological charge 2, which satisfies the theorem of Poincaré [37]. In figure 3, we observe that the "outer" surface of the stomatocyte has a higher degree of orientational order than the "inner" surface. That happens because the "inner" surface is more curved. Membrane regions with a higher absolute value of the Gaussian curvature always have a lower degree of orientational order. Regions of a vesicle membrane with small absolute values of Gaussian curvature have a higher degree of orientational order. Defects and antidefects are membrane points with a very low

degree of order, so it is not energetically favorable for them to be located in these places. As we can observe in figure 2 and figure 3, defects and antidefects always appeared in the membrane regions with high absolute values of the Gaussian curvature.

4. Conclusions

Closed biological membranes (vesicles) were considered within the spontaneous curvature model. The membrane bending energy minimization was performed to obtain ground state (zero temperature) vesicle shapes, while the Monte Carlo simulations of randomly triangulated surfaces were used to obtain membrane configurations in the thermal equilibrium (non-zero temperature). The obtained configurations, using the two approaches, correspond well with each other. In Monte Carlo simulations we did not fix the volume of the vesicle, as in the ground state calculations. Instead of that we imposed pressure difference between both membrane sides to generate vesicles with different average volumes. The vesicle had spent a relatively long "time" in the metastable oblate/discocyte state, but it later reached the equilibrium stomatocyte state, since the thermal fluctuations overcame the energy barrier. The backward transition was not observed, indicating that the stomatocyte state, if obtained, has a lower mean energy than the metastable oblate state.

The nematic ordering in oblate and stomatocyte vesicle membranes was also studied. In both cases it was confirmed that the net topological charge on surfaces with the topology of a sphere is equal 2. On an oblate vesicle, we calculated the equilibrium configuration with four topological defects, each with charge $1/2$, assembled in a region exhibiting highest Gaussian curvature. On a stomatocyte vesicle we observed six topological defects (each with charge $1/2$) and two topological antidefects (each with charge $-1/2$). The latter assembled in the region with negative Gaussian curvature. The position of topological defects is strongly curvature dependent and can be controlled by changing the vesicle curvature.

References

[1] Alberts B, Johnson A, Lewis J, Raff M, Roberts K and Walter P 2008 *Molecular biology of the cell* (Garland Science)
[2] Gao H J, Shi W D and Freund L B 2005 *Proc. Nat. Acad. Sci. USA* **102** 9469–9474
[3] Doherty G J and McMahon H T 2009 *Annu. Rev. Biochem.* **78** 857–902
[4] Sackmann E 1990 *Can. J. Phys.* **68** 999–1012
[5] Lipowsky R and Sackmann E 1995 *Structure and Dynamics of Membranes: I. From Cells to Vesicles/II. Generic and Specific Interactions* (Elsevier)
[6] Schneider M, Jenkins J and Webb W 1984 *Biophys. J.* **45** 891–899
[7] Deuling H J and Helfrich W 1976 *Biophys J.* **16** 861–868
[8] Kralj-Iglič V, Babnik B, Gauger D R, May S and Iglič A 2006 *J. Stat. Phys.* **125** 727–752
[9] Kabaso D, Bobrovska N, Góźdź W, Gov N, Kralj-Iglič V, Veranič P and Iglič A 2012 *J. Biomech.* **45** 231–238
[10] Vitelli V and Turner A M 2004 *Phys. Rev. Lett.* **93** 215301
[11] Nelson D R 2002 *Nano Lett.* **2** 1125–1129
[12] MacKintosh F and Lubensky T 1991 *Phys. Rev. Lett.* **67** 1169
[13] Kralj S, Rosso R and Virga E G 2011 *Soft Matter* **7** 670–683
[14] Selinger R L B, Konya A, Travesset A and Selinger J V 2011 *J. Phys. Chem. B* **115** 13989–13993
[15] Nguyen T S, Geng J, Selinger R L and Selinger J V 2013 *Soft Matter* **9** 8314–8326
[16] Bates M A, Skačej G and Zannoni C 2010 *Soft Matter* **6** 655–663
[17] Vitelli V and Nelson D R 2006 *Phys. Rev. E* **74** 021711
[18] Fernández-Nieves A, Vitelli V, Utada A S, Link D R, Márquez M, Nelson D R and Weitz D A 2007 *Phys. Rev. Lett.* **99** 157801
[19] Mesarec L, Fošnarič M, Penič S, Kralj-Iglič V, Kralj S, Góźdź W and Iglič A 2014 *Adv. in Soft Matter* (in print)
[20] Helfrich W 1973 *Z. Naturforsch.* **28** 693–703
[21] Evans E A 1974 *Biophys. J.* **14** 923–931
[22] Shi Z and Baumgart T 2014 *Adv. Colloid Interface Sci.* **208** 76–88

[23] Boulbitch A, Simson R, Simson D, Merkel R, Häckl W, Bärmann M and Sackmann E 2000 *Phys. Rev. E* **62** 3974
[24] Canham P B 1970 *J. of Theor. Biol.* **26** 61–76
[25] Genova J, Zheliaskova A and Mitov M 2006 *Coll. Surf. A* **282-283** 420–422
[26] Pavlič J, Genova J, Zheliaskova A, Iglič A and Mitov M 2010 *J. Phys. Conf. Ser.* **253** 012064
[27] Genova J, Kralj-Iglič V, Iglič A, Marinov R and Bivas I 2012 *J. Phys. Conf. Ser.* **398** 012037
[28] Genova J 2013 *Advances in Planar Lipid Bilayers and Liposomes* vol 17 (Academc Press, London) pp 1–27
[29] Vitkova V, Mitkova D, Stoyanova-Ivanova A, Kozarev N and Bivas I 2012 *C.R. Acad. Bulg. Sci.* **65** 329–334
[30] Dimova R 2014 *Adv. Colloid Interface Sci.* **208** 225–234
[31] Góźdź W T 2005 *J. Phys. Chem. B* **109** 21145–21149
[32] Góźdź W T 2004 *Langmuir* **20** 7385–7391
[33] Góźdź W T 2006 *J. Phys. Chem. B* **110** 21981–21986
[34] Vitelli V and Nelson D R 2006 *Phys. Rev. E* **74** 021711
[35] Rosso R, Virga E G and Kralj S 2012 *Continuum Mech. Thermodyn.* **24** 643–664
[36] Kamien R D 2002 *Rev. Mod. Phys.* **74** 953–971
[37] Poincaré H 1886 *J. Math. Pures Et Appl.* **2** 151–217
[38] Gompper G and Kroll D M 2004 *Statistical Mechanics of Membranes and Surfaces* ed Nelson D, Piran T and Weinberg S (World Scientific, Singapore) pp 359–426 2nd edition
[39] Gompper G and Kroll D M 1996 *J. de Physique I* **6** 1305–1320
[40] Ramakrishnan N, Kumar P B S and Ipsen J H 2011 *Macromol. Theory Simul.* **20** 446–450 ISSN 1521-3919
[41] Noguchi H and Gompper G 2004 *Phys. Rev. Lett.* **93** 258102
[42] Noguchi H and Gompper G 2005 *Phys. Rev. E* **72** 011901
[43] Seifert U, Berndl K and Lipowsky R 1991 *Phys. Rev. A* **44**(2) 1182–1202
[44] Bahrami A H, Raatz M, Agudo-Canalejo J, Michel R, Curtis E M, Hall C K, Gradzielski M, Lipowsky R and RWeikl T 2014 *Adv. Colloid Interface Sci.* **208** 214–224